Molecular Genetics and Metabolism Reports 42 (2025) 101193

Contents lists available at ScienceDirect

Molecular Genetics and Metabolism Reports

journal homepage: www.elsevier.com/locate/ymgmr

FBN2 pathogenic mutation in congenital contractural arachnodactyly with severe skeletal manifestations

Yazhou Huang [a,1], Xingxin Fang [a,1], Linya Ma [a], Jibo Zhang [a], Chao Wang [a], Taoran Gao [b], Dan Peng [a,*]

[a] Department of Medical Genetics, Changde Hospital, Xiangya School of Medicine, Central South University (The First People's Hospital of Changde City), 818 Renmin Road, Wuling District, Changde, Hunan 415000, China
[b] Hengyang Medical School, University of South China, Hengyang 421000, China

ARTICLE INFO

Keywords:
Congenital contractural arachnodactyly
FBN2
Whole-exome sequencing
Sanger sequencing
Splicing

ABSTRACT

Background: Congenital contractural arachnodactyly (CCA) is a rare autosomal dominant connective tissue disorder caused by mutations in the fibrillin-2 *(FBN2)* gene, characterized by crumpled ears, arachnodactyly, camptodactyly, dolichostenomelia, large-joint contractures and thoracolumbar scoliosis. Variations in the *FBN2* gene primarily include missense mutations and splice sites mutations. It is crucial to clarify whether missense mutations in the *FBN2* gene affect mRNA splicing.

Methods: We identified a novel pathogenic missense variant (c.3472G > C, p.Asp1158His) in exon 26 of the *FBN2* gene using whole-exome sequencing (WES) and Sanger sequencing. In vitro, both the wild-type and mutant minigenes were successfully inserted into the pcMINI and pcMINI-C vectors to verify the impact of this variant on *FBN2* mRNA splicing. We utilized CLUSTALW to perform multiple sequence alignment to compare the evolutionary conservation of this variant and employed AlphaFold2 to predict the protein structure of the mutant.

Results: The likely pathogenic missense mutation (c.3472G > C) results in the amino acid at position 1158 of the *FBN2* changing from aspartic acid (Asp) to histidine (His). Furthermore, DNA multiple sequence alignment indicates that this site is highly evolutionarily conserved. Functional assays and structure prediction indicated that the missense variant located at the edge of exon 26 of *FBN2* does not affect RNA splicing, instead, it changes the structure and function of the protein by altering the amino acid sequence.

Conclusion: This study enriches the pathogenic spectrum of CCA. Our research provides new insights for the diagnosis of CCA and may have an impact on genetic counseling.

1. Introduction

Congenital contractural arachnodactyly (MIM #121050) is a rare autosomal dominant connective tissue disorder that was first reported in 1971. It is characterized by abnormalities in the skeletal, cardiovascular, ophthalmic and gastrointestinal systems [1]. The primary clinical manifestations of CCA disease include crumpled ears, arachnodactyly, congenital joint contractures, kyphoscoliosis, pectus deformity, dolichostenomelia, muscle hypoplasia, micrognathia [2,3]. CCA and Marfan syndrome (MFS, MIM #154700) share many skeletal features, known as a Marfanoid appearance, but the incidence of CCA is significantly lower than that of MFS [4].

CCA is caused by pathogenic variants in *FBN2*, which is located on chromosome 5q23.3 [5,6]. *FBN2* contains 65 exons, and disease-associated variants are predominantly found in central stretch of calcium-binding epidermal growth factor-like (cbEGF-like) domains (exons 24–35) [7,8]. It encodes fibrillin-2 which contains 2912 amino acids and is expressed during early embryonic development. This protein polymerizes into linear structures called microfibrils and provides support for elastic and non-elastic connective tissues [9,10]. Pathogenic variants in *FBN2* can alter the structure of fibrillin-2, leading to its dysfunction, resulting in reduced microfibril formation and decreased fiber flexibility, thereby causing the clinical symptoms of CCA [11]. Fibrillin-1 and fibrillin-2 are widely distributed throughout the human body from embryonic stages, indicating that these two glycoproteins play multiple roles in the organogenesis process [12]. Up until July 7,

* Corresponding author.
E-mail address: dasan0988@126.com (D. Peng).
[1] These authors contributed equally to this work.

https://doi.org/10.1016/j.ymgmr.2025.101193
Received 6 November 2024; Received in revised form 13 January 2025; Accepted 14 January 2025

2024, only 268 different types of variants in the *FBN2* gene have been reported in the Human Gene Mutation Database (HGMD), and the clinical significance of some variations remains unknown. RNA splicing is the process of removing introns from pre-mRNA and joining exons in an orderly fashion to ultimately produce mature mRNA, which plays a vital role in gene expression [13]. This process is dependent on the presence of conserved nucleotides at the intron-exon boundaries and branch point sequences slightly upstream from the 3′ splice site. Analysis using skin fibroblasts from the CCA patient indicates that the expression level of the *FBN2* allele with the exon 29 deletion inherited from the father is higher than that of the maternally inherited allele, which the splicing error resulted from an A-to-G transition 15 nt upstream from the 3′ splice site of the intron 28 and resulted in disrupt one of the 43 calcium-binding EGF-like domains of the fibrillin-2 protein[14]. These results suggest that aberrant splicing of *FBN2* exons may cause CCA, providing insight into the molecular basis of this disease [14]. Mice with a targeted deletion of fibrillin-2 gene (*Fbn2*) were generated using gene targeting techniques, resulting in the observation of bilateral syndactyly-like limb pattern defects [11]. Recent studies have shown that fibrillin-2 protein is involved in regulating the deposition of elastin in adult skin models, and that hypoxia specifically affects the elastin network without impacting the collagen and fibronectin networks [15]. The minigene technique has become a primary method for studying and identifying cis-elements and trans-factors that regulate tissue-specific alternative splicing. This technique involves cloning relevant genomic fragments upstream of a common transcriptional promoter and downstream of necessary gene fragments at the 3′ end of mRNA, all within a plasmid [16].

Here, we report a case where a novel *FBN2* missense mutation c.3472G > C (p.Asp1158His) causing congenital contractural arachnodactyly was identified through whole exome sequencing. Sanger sequencing was performed, confirming it as a de novo mutation, since this variant was not detected in the parents. The variant was located at the edge of exon 26 of *FBN2* which might be expected to affect mRNA splicing and a number of tools predicted that it would affect splicing. However, minigene experiments indicated that this missense variant did not affect RNA splicing. The p.Asp1158His mutation changed the amino acid at position 1158 from acidic to basic and disrupted the hydrogen bond formed with Asn1176, thereby potentially changing the function of the protein. This discovery illustrates that when clinical analysts interpret whole-exome sequencing results, the pathogenicity of genetic variants predicted by tools may not align with actual outcomes. This finding underscores the need for functional genetic experiments to validate the etiologies of genetic variants, supporting clinical analysis of whole exome sequencing results.

2. Materials and methods

2.1. Patient consent and ethics statement

Written informed consent was obtained from each subject or their guardians for participation in this study. The study was conducted according to the guidelines of the Declaration of Helsinki, and approved by the Ethics Committee of the First People's Hospital of Changde City (protocol code 2024-189-01) on July 24, 2024.

2.2. Whole Exome Sequencing and bioinformatic analysis

Genomic DNA was extracted from proband's peripheral blood with a Qiagen DNA Blood Midi/Mini kit (Qiagen GmbH, Hilden, Germany) following the manufacturer's protocol. DNA was fragmented to approximately 200 bp, followed by end repaired and the addition of a single A base to the 3'end. After PCR amplification, the DNA fragments were hybridized and captured using the Nano WES Human Exome V1 (Berry Genomics) according to the manufacturer's protocol. Novaseq6000 platform (Illumina, San Diego, USA) was employed with 150 bp pair-end sequencing mode. Raw image files were processed using CASAVA v1.82 for base calling and generating raw data. The sequencing reads were aligned to the human reference genome (hg38/GRCh38) using the Burrows–Wheeler Aligner tool, and PCR duplicates were removed by using Picard v1.57 (http://picard.sourceforge.net/). Verita Trekker® Variants Detection System by Berry Genomics and the third-party software GATK (https://software.broadinstitute.org/gatk/) were employed for variant calling.[17] All variants were screened against population databases, including the Exome Aggregation Consortium (ExAC http://exac.broadinstitute.org/) and gnomAD (http://gnomad.broadinstitute.org/). SIFT(http://sift.jcvi.org), PolyPhen-2 (http://genetics.bwh.harvard.edu/pph2), CADD (https://cadd.gs.washington.edu), and Rare Exome Variant Ensemble Learner (REVEL) (https://sites.google.com/site/revelgenomics/) were used for pathogenicity prediction. We referred to disease and phenotype information from databases, including OMIM database(http://www.omim.org), ClinVar-database (http://www.ncbi.nlm.nih.gov/clinvar) and Human Gene Mutation Database (http://www.hgmd.org). The variants were classified into five categories, pathogenic (P), likely pathogenic (LP), uncertain significance (VUS), likely benign (LB) and benign (B), according to the American College of Medical Genetics and Genomics (ACMG) guidelines [18].

Table 1
Primers F and R represent the forward primer and reverse primer, respectively.

Primer	Primer sequence(5′-3′)
197,530-F	aggagatttctcagagaacc
197,778-F	gcctgtctctctgggggtttg
199,864-R	gagaccacaaggacttccac
200,125-R	aaagcaataggttgcaacgc
pcMINI-FBN2-KpnI-F	ggtaGGTACCtctgtcacccaggctggagt
pcMINI-FBN2-XhoI-R	tttcCTCGAGgaatcttagacttataacct
pcMINI-C-FBN2-KpnI-F	ggtaGGTACCtggggtctccctacattgcc
pcMINI-C-FBN2-XhoI-R	TAGACTCGAGatCCACACAGTCCTCACGGGAT
FBN2-mut-F	ATGAAGAACTGCATGCgtaagcaccgtgagc
FBN2-mut-R	gctcacggtgcttacGCATGCAGTTCTTCAT
pcMINI-C-F	CTAGAGAACCCACTGCTTAC
pcMINI-C-R	TAGAAGGCACAGTCGAGG
pcMINI-F	CTAGAGAACCCACTGCTTAC
pcMINI-R	TAGAAGGCACAGTCGAGG

2.3. Mutation validation by sanger sequencing

Primers were designed using Primer 5 based on the DNA fragments that needed to be sequenced. The sequences of the *FBN2* primers were *FBN2*-Forward: 5′-ATGCAGCACCTTCGCTTG-3′ and *FBN2*-Reverse:5′-TAAATCTCTTCTCTCTCTCACCACA-3′. PCR products were purified and sequenced using an ABI 3730 DNA Analyzer with the BigDye™ Terminator Cycle Sequencing Kit (Applied Biosystems, Foster, CA, USA).

2.4. Minigene splicing assays

Firstly, we designed two sets of nested primers, 197,530-F and 199,864-R, and 197,778-F and 200,125-R (primers in Table 1), for nested PCR using normal human DNA as a template. Using the product from nested PCR as a template, the wild-type fragment 1 (1124 bp), was amplified with the primers pcMINI-FBN2-*Kpn*I-F and pcMINI-FBN2-*Xho*I-R. Next, we used the nested PCR product as a template, the left half of the mutated fragment (659 bp), was amplified with the primers pcMINI-FBN2-KpnI-F and FBN2-mut-R, and the right half of the mutated fragment (496 bp) was amplified with the primers pcMINI-FBN2-XhoI-R and FBN2-mut-F. We mixed the mutated left and right halves in a 1:1 ratio as a template and used pcMINI-FBN2-KpnI-F and pcMINI-FBN2-XhoI-R as primers to amplify the mutant fragment 1(1124 bp). Moreover, we used similar methods and corresponding primers to obtain wild-type fragments 2 and mutant fragments 2 (1470 bp) (primers in Table 1). Then, after amplification, the vectors pcMINI and pcMINI-C

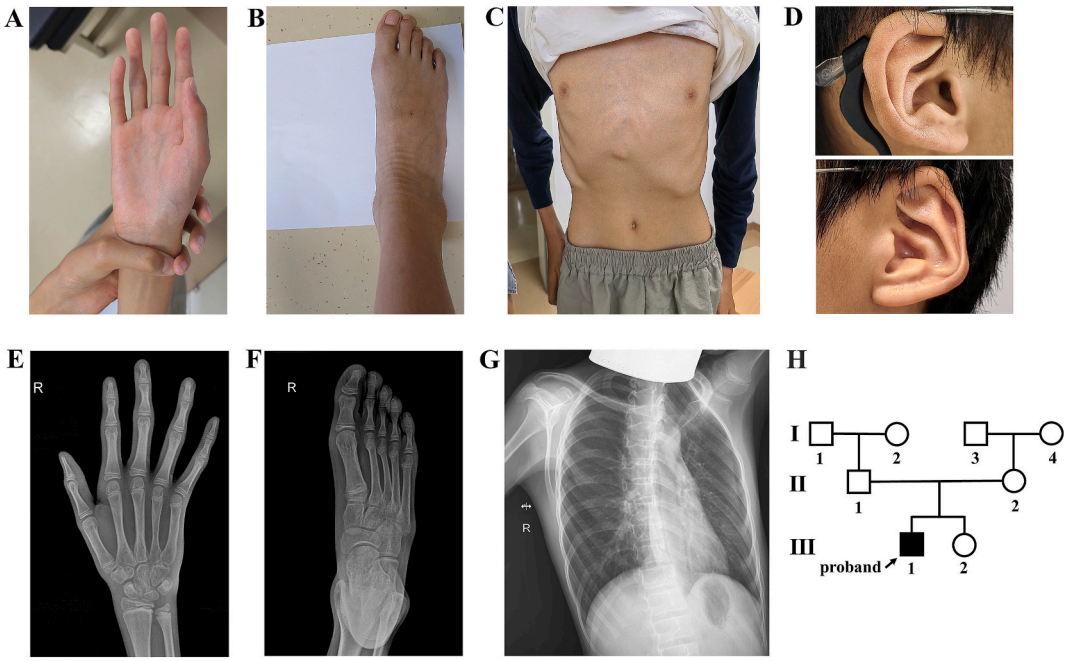

Fig. 1. Clinical features of proband and pedigree information. (A) (B) Photographs of the right hand and right root. (C) Photograph of the thorax. (D) Photographs of the left ear and right ear. (E) (F) X-ray of the right hand and right root of the proband. (G)X-ray of the thorax. (H) Pedigree of this CCA family. Filled symbols marked with black numbers represent individuals affected by CCA; open symbols marked with black numbers represent wild-type individuals. Circles and squares indicate females and males, respectively.

which have been optimized in our laboratory, as well as their fragments, were subjected to digestion, purification, ligation, transformation, colony PCR identification, and Sanger sequencing (primers in Table 1). The wild-type fragments 1 and mutant fragments 1 containing part of intron 25 (505 bp), exon 26 (129 bp), and part of intron 26 (470 bp) were constructed into the pcMINI vectors which contains the splicing pattern of ExonA-Exon26-ExonB. The wild-type 2 fragments and mutant fragments 2 of intron25 (383 bp)-Exon26(129 bp)-intron26(810 bp)-Exon27(126 bp) were constructed into the pcMINI-C vectors, which contains a universal ExonA-intronA-MCS. Subsequently, because of the patient's refusal to collect skin cells for the preparation of fibroblasts, four types of recombinant vectors were constructed and transfected into the HeLa and 293 T cell lines, following the guidelines specified in the lipofection manual. After transfection for 48 h, the cells were collected to extract total RNA and then reverse transcribed into cDNA. Finally, we used the primers pcMINI-F/pcMINI-R to amplify pcMINI-wild type (wt)/mutation (mut), and the primers pcMINI-C-F/pcMINI-C-R to amplify pcMINI-C-wild type (wt)/mutation (mut) (primers in Table 1). We carried out agarose gel electrophoresis for the separation of the amplified products and proceeded with Sanger sequencing.

2.5. Conservation analysis and protein structural modeling

Firstly, we download the fibrillin-2 protein sequences for various species from the Ensembl website(https://asia.ensembl.org/index.html). Next, we used the online tool CLUSTALW (https://www.genome.jp/tools-bin/clustalw) for sequence alignment, and then use BioEdit for visualization. We used the AlphaFold2 protein structure database (https://alphafold.ebi.ac.uk/) to generate structural models of the fibrillin-2 protein. Lastly, protein structure visualization was achieved using PyMOL version 2.6.0 open-source copyright.

Table 2
Clinical CCA scoring system [adapted from [3]]. (Pts: points).

Clinical feature	Points	Proband (III:1)	Father (II:1)	Mother (II:2)
Crumpled ears	3	3	0	0
Arachnodactyly	3	3	0	0
Camptodactyly	3	3	0	0
Large-joint contractures	3	3	0	0
Pectus deformity	2	2	0	0
Dolichostenomelia	2	1	0	0
Kyphoscoliosis	1	0	0	0
Muscle hypoplasia	1	0	0	0
High palate	1	0	0	0
Micrognathia	1	0	0	0
Total Score (>7 pts., CCA likely)	20	15	0	0

3. Results

3.1. Clinical characteristics

The parents were unrelated, healthy, and did not receive medical attention until they delivered the proband (Fig. 1(H) III-1) who is an 11-year-old boy affected by arachnodactyly, contractures of large joints, camptodactyly (Fig. 1(A B E F)), pectus deformity (Fig. 1(C G)), dolichostenomelia, nearsightedness, crumpled ears (Fig. 1(D)). Moreover, according to the CCA clinical scoring system[3], the proband's score is 15 points (Table 2). The proband has a history of a left femur fracture at 3 months of age. His height and weight were 161 cm and 33.5 kg, respectively, and his arm span was 165.6 cm (span/height = 1.03). Otherwise, no issues have been found on the cardiac ultrasound, and the proband's intelligence is normal. Other members of the family were asymptomatic and not associated with CCA.

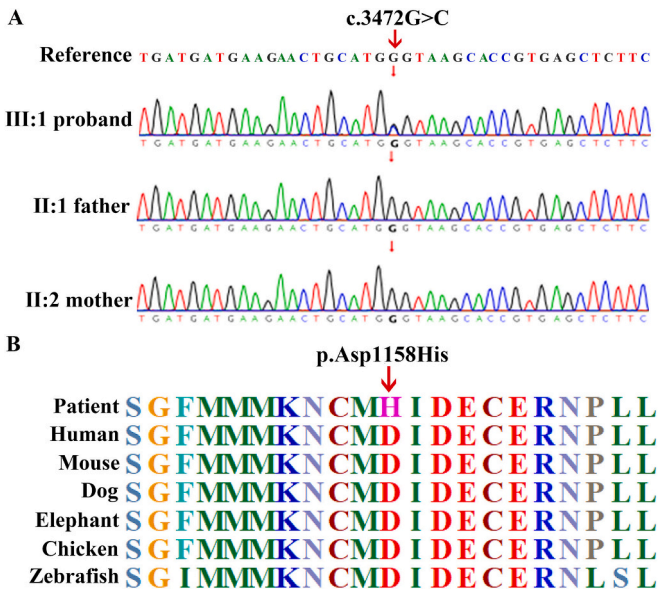

Fig. 2. *FBN2* variant analysis of the pedigree. (A) The Sanger sequencing of the pedigree, red arrow indicates mutation site. (B) the evolutionary conservation across multiple species clusters, red arrow indicates mutation site.

3.2. Variant identification and bioinformatic analysis

To determine the genetic cause of the CCA case, peripheral blood was drawn from the proband and his parents for whole exome sequencing (WES) and family verification. We found a novel heterozygous variant in exon 26 of the *FBN2* gene (hg38 chr5:128338933G/C, NM_001999.4, c.3472G > C, p.Asp1158His) in the proband (Fig. 2A). We found that this variant is not recorded in the two public databases: the Exome Sequencing Project(https://evs.gs.washington.edu/EVS/) and gnomAD databases. The variant was predicted to be deleterious by MutationTaster(https://www.mutationtaster.org/), with a PhyloP score of 6.033 and a PhastCons score of 1. PolyPhen-2(http://genetics.bwh.harvard.edu/pph2/) and VarCards(http://www.genemed.tech/varcards/) predicted the variant to be probably damaging, with scores of 1 and 0.96, respectively. Additionally, the splice prediction tools SpliceAI(https://spliceailookup.broadinstitute.org/) with scores of 0.5 and Fruitfly(https://www.fruitfly.org/seq_tools/splice.html) with the confidence score of the original donor site decreased by 0.11, suggest that this mutation may affect mRNA splicing.

3.3. Mutation validation by sanger sequencing

Sanger sequencing indicated that the *FBN2* variant c.3472G > C was not detected in the proband's parents (II-1 and II-2), indicating it is a de novo mutation. In summary, the variant was classified as likely

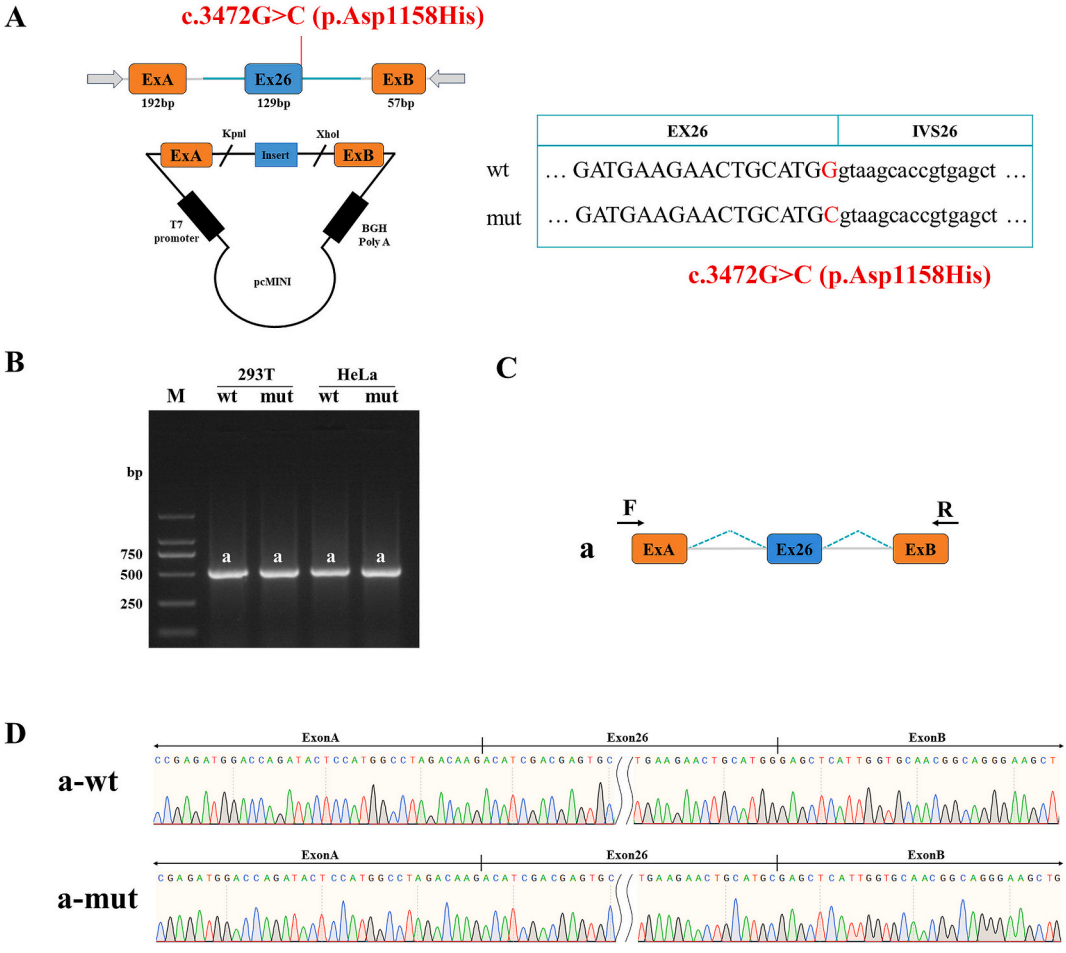

Fig. 3. Results of pcMINI vector detection: (A) Schematic diagram of minigene construction strategy, with wt (wild type) displayed above and mut (mutation) below. A segment containing part of intron 25 (505 bp), exon 26 (129 bp), and part of intron 26 (470 bp) of *FBN2* gene was inserted into the pcMINI vector, which contains the splicing pattern of ExonA-Exon26-ExonB. Ex stands for the exon, and the line in front of the exon represents the intron. (B) Gel electrophoresis and splicing diagrams of RT-PCR transcripts, with bands labeled as a in HeLa and 293 T cells. (C) Schematic diagram of minigene splicing. (D) Sequencing results corresponding to the splicing bands, both the wild-type and mutant splicing patterns are shown in a.

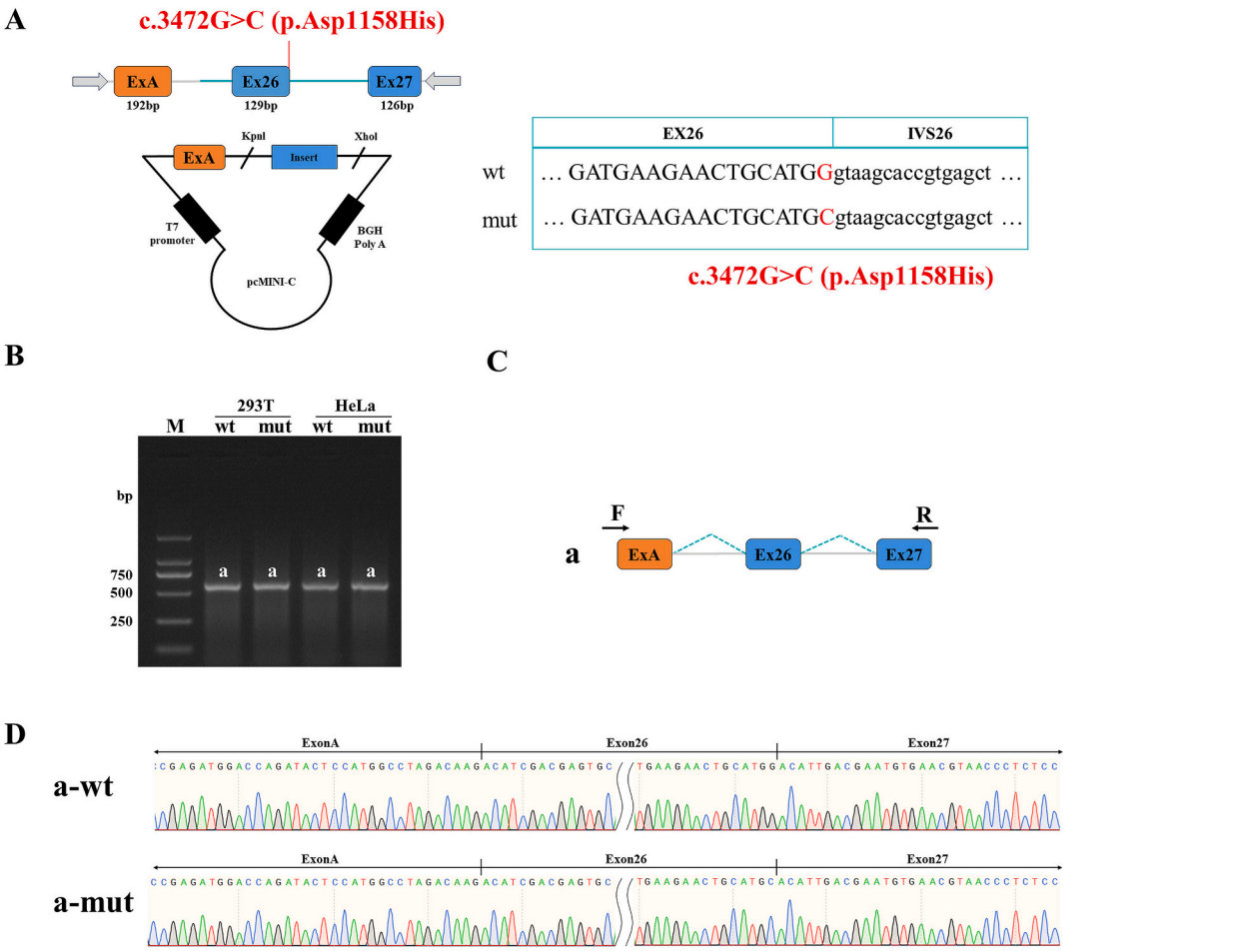

Fig. 4. Results of pcMINI-C vector detection: (A) Schematic diagram of minigene construction strategy, with wt (wild type) displayed above and mut (mutation) below. A segment of intron25 (383 bp)-Exon26(129 bp)-intron26(810 bp)- Exon27(126 bp) of *FBN2* gene was inserted into the pcMINI-C vector, which contains a universal ExonA-intronA-MCS. Ex stands for the exon, and the line in front of the exon represents the intron. (B) Gel electrophoresis and splicing diagrams of RT-PCR transcripts, with bands labeled as a in HeLa and 293 T cells. (C) Schematic diagram of minigene splicing. (D) Sequencing results corresponding to the splicing bands, both the wild-type and mutant splicing patterns are shown in a.

pathogenic according to the ACMG 2015 guideline. Moreover, the conservation analysis revealed that c.3472G (amino acid Asp1158) of the human *FBN2* gene is highly conserved among various species, including human, mouse, dog, elephant, chicken, and zebrafish (Fig. 2B). This suggests that alterations at this site could disrupt the fibrillin-2 protein's normal function.

3.4. Minigene splicing assays

Since the missense mutation is located at the edge of exon 26 in the FBN2 gene, and the SpliceAI and Fruitfly software predict that it may affect mRNA splicing, we constructed a minigene to elucidate the impact of this variation on mRNA splicing. Both the wild-type and mutant minigenes were successfully inserted into vectors pcMINI and pcMINI-C, as shown in Fig. 3A and C and Fig. 4A and C, generating four recombinant vectors which were transfected into HeLa and 293 T cell lines. RT-PCR experiment showed that in HeLa and 293 T cells, the wild-type appeared as a single band, designated band a, which was consistent with the expected size (518 bp) (Fig. 3B). Moreover, the mutant type in HeLa and 293 T cells also appeared as a single band, consistent in size with the wild-type band, designated as band a. Sanger sequencing of the wild-type and mutant bands from both cell lines indicated that both the wild-type band a and the mutant band a were normal splicing bands with the splicing pattern of ExonA(192 bp)-Exon26(129 bp)-ExonB (57 bp) (Fig. 3D).

After transfection into cells, the splicing pattern of ExonA-Exon26-Exon27 (Fig. 4C) was observed for any abnormalities. RT-PCR detection results indicated that in HeLa and 293 T cells, the wild-type was a single band, consistent with the expected size (595 bp), as shown in Fig. 4B, named band "a". In HeLa and 293 T cells, the mutant type was also a single band and consistent in size with the wild-type band, also named band "a". Sequencing results indicate that both the wild-type band a and the mutant band "a" are normally spliced bands, with the splicing pattern of ExonA(192 bp)-Exon26(129 bp)- Exon27(126 bp), as shown in Fig. 4D.

All in all, the minigenes in vitro experimental results indicate that the missense mutation (c.3472G > C p.Asp1158His) does not affect the normal splicing of the gene's mRNA, and the detection results of the two sets of vectors, pcMINI and pcMINI-C, are consistent, indicating it might change the function of the protein by altering the amino acid sequence.

3.5. Protein structure analysis

We used the AlphaFold2 software to predict the structure of the fibrillin-2 protein mutation containing the altered amino acid. The overall structure of the mutant shows no significant changes compared to the wild-type structure. The p.Asp1158His mutation changed the property of the amino acid from acidic to basic, but did not alter the hydrophobicity of the amino acid. Compared to the wild-type protein, the amino acid Asp1158 mutated to His1158, which disrupts the

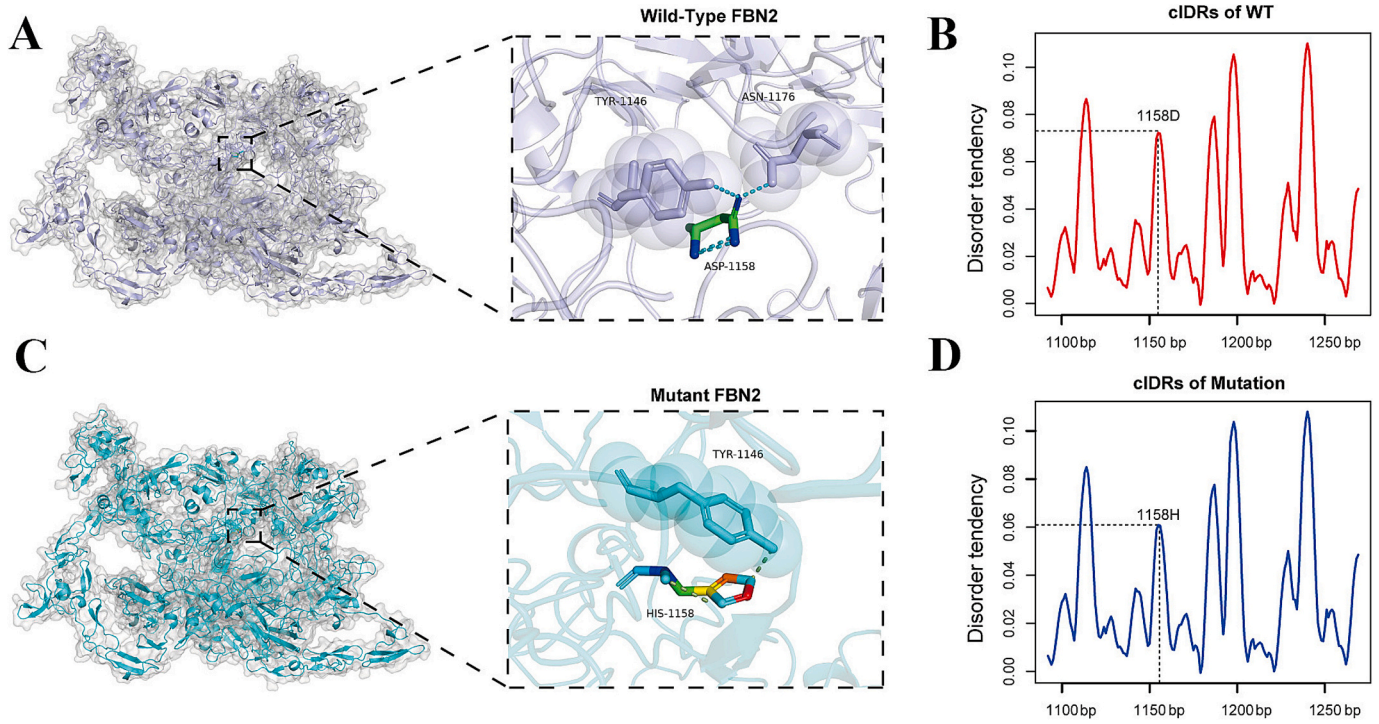

Fig. 5. Protein structural modeling analysis and schematic representation of fibrillin-2 protein. (A) Three-dimensional model and enlarged image of residues of Asp1158 in wild-type fibrillin-2. (B) disorder plot of wild-type fibrillin-2 predicted by IUPred. (C) Three-dimensional model and enlarged image of residues of His1158 in mutant fibrillin-2. (D) disorder plot of mutant fibrillin-2 predicted by IUPred.

hydrogen bond between Asp1158 and Tyr1146 and Asn1176, while His1158 forms a new hydrogen bond with Tyr1146 (Fig. 5A and Fig. 5C). The p.Asp1158His mutation likely reduces disorder in the protein's core region, which may affect its binding activity (Fig. 5B and Fig. 5D).Therefore, this amino acid appears to play a crucial role in the structure and function of fibrillin-2 protein.

4. Discussion

Pathogenic variants of the *FBN2* gene are associated with CCA, with most pathogenic mutations concentrated in exons 24 to 35 (the central region of the gene encoding multiple EGF-like domains), with pathogenic mutations primarily being missense and splice-site variants [6]. A novel potentially pathogenic missense mutation in the FBN2(p.Gly1145Asp) has been identified, which causes a substitution from hydrophobic to hydrophilic of the amino acid, resulting in a change from neutral to acidic amino acid properties, potentially leading to alterations in the protein's three-dimensional structure [19]. A novel multiexon deletion of exons 35–39 (no hot spot) in *FBN2* was identified by copy number variation sequencing, which result in an in-frame loss of exons 35–39 and produce an internally truncated fibrillin-2 protein [20]. Previous studies have also identified deletions within the *FBN2* that can express a truncated protein without the normal function of the fibrillin-2 protein [21,22]. Interestingly, deletions of exons 1–8 in the *FBN2* gene have been found in healthy individuals [21]. These studies indicated that the dominant-negative effect of *FBN2* mutants on the wild-type protein, rather than haploinsufficiency, represents a potential pathological mechanism [7,23].

A number of previous studies have shown that splice site variants in *FBN2* can cause CCA due to haploinsufficiency. Currently, the HGMD database records 28 mutations at the splicing sites of the *FBN2* gene, most of which are classic splicing mutations. A new mutation, c.3724 + 1G > A, was identified at the donor splice site of intron 28 in the *FBN2* gene, leading to the disruption of the splice site sequence, with predictions suggest that exon 28 is skipped [24]. In a family, nine patients were found to have the *FBN2* c.3724 + 3 A > C variation, leading to an in-frame deletion during transcription and ultimately causing congenital contractural arachnodactyly [25]. A *FBN2* pathogenic variant in congenital contractural arachnodactyly with a severe cardiovascular phenotype was identified by whole-exome sequencing, Sanger sequencing and RNA sequencing, resulting in the exon 35 skipping [26]. Additionally, two missense mutations in the *FBN2* gene that affect splicing have been documented [27,28]. In this study, multiple in silico tools for predicting the pathogenicity of genetic variants have suggested that the missense mutation located at the edge of exon 26 in the *FBN2* gene could affect splicing. By constructing the *FBN2* minigene in two sets of vectors, pcMINI and pcMINI-C, transcription analysis results indicated that the mutation (c.3472G > C p.Asp1158His) does not affect normal mRNA splicing. We found that the c.3472G > C (p.Asp1158His) mutation alters the aspartic residue and consequently modifies the cbEGF domain, which would potentially disrupt the disulfide bonds and thereby disrupt the natural folding of fibrillin-2 protein. The study results suggest that when analyzing whole-exome sequencing results, the predictions made by in silico tools for predicting the pathogenicity of genetic variants may not always be accurate, and it is crucial to verify them with functional genetic experiments when necessary.

5. Conclusion

In conclusion, our study identified a novel *FBN2* mutation (c.3472G > C) in a three-generation family, confirming that this mutation is highly likely to be the genetic cause of CCA in this family. Our research has expanded the disease spectrum of CCA.

Author's contributions statement

Yazhou Huang and Xingxin Fang designed the research; Yazhou Huang, Linya Ma, Jibo Zhang, Chao Wang and Taoran Gao performed the research; Yazhou Huang analyzed the data and wrote the manuscript; Yazhou Huang and Dan Peng revised the manuscript.

Funding

This work was supported by Hunan Provincial Natural Science Foundation of China (2024JJ7014) and the Science and Technology Innovation Program of Changde City (2023ZD65).

Ethics approval and consent to participate

Written informed consent was obtained from each subject or their guardians for participation in this study. The study was conducted according to the guidelines of the Declaration of Helsinki, and approved by the Ethics Committee of the first people's hospital of Changde city (protocol code 2024–189-01) on July 24, 2024.

Consent for publication

Consent for publication was obtained from parents of all the enrolled patients.

Declaration of competing interest

The authors declare no conflicts of interest.

Acknowledgements

We are grateful to all patients and their families who participated in this study.

Data availability

The datasets used and/or analyzed during the current study are available from the corresponding author on reasonable request.

References

[1] R.K. Beals, F. Hecht, Congenital contractural arachnodactyly: a heritable disorder of connective tissue, JBJS 53 (1971) 987–993.
[2] X. Guo, C. Song, Y. Shi, H. Li, W. Meng, Q. Yuan, J. Xue, J. Xie, Y. Liang, Y. Yuan, Whole exome sequencing identifies a novel missense FBN2 mutation co-segregating in a four-generation Chinese family with congenital contractural arachnodactyly, BMC Med. Genet. 17 (2016) 1–5.
[3] I. Meerschaut, S. De Coninck, W. Steyaert, A. Barnicoat, A. Bayat, F. Benedicenti, S. Berland, E.M. Blair, J. Breckpot, A. De Burca, A clinical scoring system for congenital contractural arachnodactyly, Genet. Med. 22 (2020) 124–131.
[4] A.J. Macnab, L. D'Orsogna, D. Cole, P.E. Baguley, R.J. Adderley, M. Patterson, Cardiac anomalies complicating congenital contractural arachnodactyly, Arch. Dis. Child. 66 (1991) 1143–1146.
[5] B. Callewaert, Congenital Contractural Arachnodactyly, 2022.
[6] M.Y. Frédéric, C. Monino, C. Marschall, D. Hamroun, L. Faivre, G. Jondeau, H. G. Klein, L. Neumann, E. Gautier, C. Binquet, The FBN2 gene: new mutations, locus-specific database (universal mutation database FBN2), and genotype-phenotype correlations, Hum. Mutat. 30 (2009) 181–190.
[7] P.A. Gupta, E.A. Putnam, S.G. Carmical, I. Kaitila, B. Steinmann, A. Child, C. Danesino, K. Metcalfe, S.A. Berry, E. Chen, Ten novel FBN2 mutations in congenital contractural arachnodactyly: delineation of the molecular pathogenesis and clinical phenotype, Hum. Mutat. 19 (2002) 39–48.
[8] S. Zhou, F. Wang, Y. Dou, J. Zhou, G. Hao, C. Xu, Q.K. Wang, H. Wang, P. Wang, A novel FBN2 mutation cosegregates with congenital contractural arachnodactyly in a five-generation Chinese family, Clin. Case Reports 6 (2018) 1612.
[9] J. Olivieri, S. Smaldone, F. Ramirez, Fibrillin assemblies: extracellular determinants of tissue formation and fibrosis, Fibrogenesis Tissue Repair 3 (2010) 1–8.
[10] S. Peeters, A. Decramer, S.A. Cain, P. Houpt, F. Verstreken, J. Noyez, C. Hermans, W. Jacobs, M. Lammens, E. Fransen, Delineation of a new fibrillin-2-opathy with evidence for a role of FBN2 in the pathogenesis of carpal tunnel syndrome, J. Med. Genet. 58 (2021) 778–782.
[11] E. Arteaga-Solis, B. Gayraud, S.Y. Lee, L. Shum, L. Sakai, F. Ramirez, Regulation of limb patterning by extracellular microfibrils, J. Cell Biol. 154 (2001) 275–282.
[12] F. Quondamatteo, D.P. Reinhardt, N.L. Charbonneau, G. Pophal, L.Y. Sakai, R. Herken, Fibrillin-1 and fibrillin-2 in human embryonic and early fetal development, Matrix Biol. 21 (2002) 637–646.
[13] S.C. Bonnal, I. López-Oreja, J. Valcárcel, Roles and mechanisms of alternative splicing in cancer—implications for care, Nat. Rev. Clin. Oncol. 17 (2020) 457–474.
[14] E.A. Putnam, E.-S. Park, C.M. Aalfs, R. Hennekam, D.M. Milewicz, Parental somatic and germ-line mosaicism for a FBN2 mutation and analysis of FBN2 transcript levels in dermal fibroblasts, Am. J. Hum. Genet. 60 (1997) 818.
[15] J. Boizot, M. Minville-Walz, D.P. Reinhardt, M. Bouschbacher, P. Sommer, D. Sigaudo-Roussel, R. Debret, FBN2 silencing recapitulates hypoxic conditions and induces elastic fiber impairment in human dermal fibroblasts, Int. J. Mol. Sci. 23 (2022) 1824.
[16] G. Singh, T.A. Cooper, Minigene reporter for identification and analysis of cis elements and trans factors affecting pre-mRNA splicing, Biotechniques 41 (2006) 177–181.
[17] K. Wang, M. Li, H. Hakonarson, ANNOVAR: Functional annotation of genetic variants from next-generation sequencing data Nucleic Acids Research, in: ANNOVAR: Functional Annotation of Genetic Variants from Next-generation Sequencing Data Nucleic Acids Research 38, 2010.
[18] S. Richards, N. Aziz, S. Bale, D. Bick, S. Das, J. Gastier-Foster, W.W. Grody, M. Hegde, E. Lyon, E. Spector, Standards and guidelines for the interpretation of sequence variants: a joint consensus recommendation of the American College of Medical Genetics and Genomics and the Association for Molecular Pathology, Genet. Med. 17 (2015) 405–423.
[19] G. You, B. Zu, B. Wang, Z. Wang, Y. Xu, Q. Fu, Exome sequencing identified a novel FBN2 mutation in a Chinese family with congenital contractural arachnodactyly, Int. J. Mol. Sci. 18 (2017) 626.
[20] H. Yagi, H. Takiguchi, N. Takeda, R. Inuzuka, Y. Taniguchi, K.J. Porto, H. Ishiura, J. Mitsui, H. Morita, I. Komuro, Family with congenital contractural arachnodactyly due to a novel multiexon deletion of the FBN2 gene, Clin. Case Reports 10 (2022) e05335.
[21] M. Inbar-Feigenberg, N. Meirowitz, D. Nanda, A. Toi, N. Okun, D. Chitayat, Beals syndrome (congenital contractural arachnodactyly): prenatal ultrasound findings and molecular analysis, Ultrasound Obstet. Gynecol. 44 (2014) 486–490.
[22] A. Lavillaureix, S. Heide, S. Chantot-Bastaraud, I. Marey, B. Keren, R. Grigorescu, J. Jouannic, A. Gelot, S. Whalen, D. Héron, Mosaic intragenic deletion of FBN2 and severe congenital contractural arachnodactyly, Clin. Genet. 92 (2017) 556–558.
[23] W. Courtens, W. Tjalma, L. Messiaen, E. Vamos, J. Martin, E. Van Bogaert, G. Keersmaekers, P. Meulyzer, J. Wauters, Prenatal diagnosis of a constitutional interstitial deletion of chromosome 5 (q15q31. 1) presenting with features of congenital contractural arachnodactyly, Am. J. Med. Genet. 77 (1998) 188–197.
[24] V. Mehar, D. Yadav, R. Kumar, S. Yadav, K. Singh, B. Callewaert, S. Pathan, A. De Paepe, P.J. Coucke, Congenital contractural arachnodactyly due to a novel splice site mutation in the FBN2 gene, J. Pediatr. Genet. 3 (2014) 163–166.
[25] P. Xu, R. Li, S. Huang, M. Sun, J. Liu, Y. Niu, Y. Zou, J. Li, M. Gao, X. Li, A novel splicing mutation in the FBN2 gene in a family with congenital contractural arachnodactyly, Front. Genet. 11 (2020) 143.
[26] S. Yang, Z. Li, FBN2 pathogenic variants in congenital contractural arachnodactyly with severe cardiovascular manifestations, Connect. Tissue Res. (2024) 1–12.
[27] S. Renner, H. Schüler, M. Alawi, V. Kolbe, M. Rybczynski, R. Woitschach, S. Sheikhzadeh, V.C. Stark, J. Olfe, E. Roser, Next-generation sequencing of 32 genes associated with hereditary aortopathies and related disorders of connective tissue in a cohort of 199 patients, Genet. Med. 21 (2019) 1832–1841.
[28] N. Weisschuh, P. Mazzola, T. Zuleger, K. Schaeferhoff, L. Kühlewein, F. Kortüm, D. Witt, A. Liebmann, R. Falb, L. Pohl, Diagnostic genome sequencing improves diagnostic yield: a prospective single-Centre study in 1000 patients with inherited eye diseases, J. Med. Genet. 61 (2024) 186–195.